

Uncovering surface plasmon optical resonances in nanohole arrays through interferometric photoemission electron microscopy

Cite as: Appl. Phys. Lett. **120**, 081102 (2022); <https://doi.org/10.1063/5.0082481>

Submitted: 15 December 2021 • Accepted: 04 February 2022 • Published Online: 22 February 2022

Published open access through an agreement with Pacific Northwest National Laboratory

 Kevin T. Crampton,  Alan G. Joly and  Patrick Z. El-Khoury

COLLECTIONS

Paper published as part of the special topic on [Optical Nanoprobe Spectroscopy and Imaging](#)



View Online



Export Citation



CrossMark

ARTICLES YOU MAY BE INTERESTED IN

[Broadband, efficient extraction of quantum light by a photonic device comprised of a metallic nano-ring and a gold back reflector](#)

Applied Physics Letters **120**, 081103 (2022); <https://doi.org/10.1063/5.0082347>

[Broadband and high-performance SnS₂/FePS₃/graphene van der Waals heterojunction photodetector](#)

Applied Physics Letters **120**, 081101 (2022); <https://doi.org/10.1063/5.0083272>

[Improved LED output power and external quantum efficiency using InGaN templates](#)

Applied Physics Letters **120**, 081104 (2022); <https://doi.org/10.1063/5.0084273>



Characterizing nanostructures?
Learn about a new way to get high-quality data in a fraction of the time

[Read the tech note](#)

 Lake Shore
CRYOTRONICS

Uncovering surface plasmon optical resonances in nanohole arrays through interferometric photoemission electron microscopy

Cite as: Appl. Phys. Lett. **120**, 081102 (2022); doi: 10.1063/5.0082481

Submitted: 15 December 2021 · Accepted: 4 February 2022 ·

Published Online: 22 February 2022



View Online



Export Citation



CrossMark

Kevin T. Crampton,^{a)}  Alan G. Joly,  and Patrick Z. El-Khoury^{a)} 

AFFILIATIONS

Physical Sciences Division, Pacific Northwest National Laboratory, P.O. Box 999, Richland, Washington 99352, USA

Note: This paper is part of the APL Special Collection on Optical Nanoprobe Spectroscopy and Imaging.

^{a)}Authors to whom correspondence should be addressed: kevin.crampton@pnnl.gov and patrick.elkhoury@pnnl.gov

ABSTRACT

The role of surface plasmon polaritons (SPPs) in nanohole array optical extinction spectra is explored using a time-resolved technique capable of isolating the air/metal interfacial SPP contribution to the typical Fano profile in optical transmission curves. A pair of interferometrically locked broad-band femtosecond pulses is used to launch SPPs from lithographically patterned plasmonic nanohole arrays. SPPs launched in the co- and counter-propagating directions are probed using a third probe pulse in a photoemission electron microscope. Using this approach, we record interferometric SPP-SPP linear autocorrelations that selectively report on the resonances of SPPs launched from arrays of varying pitches and hole diameters. Aside from advancing an approach to selective SPP spectroscopy, we illustrate that resonant coupling in the counter-propagating direction may be exploited to control the spatial, temporal, and spectral characteristics of SPPs. For the counter-propagating direction, we show that tuning the array pitch near the fundamental plasmon resonance generates color-tuned (~ 770 – 820 nm), narrow bandwidth SPPs, and the bandwidth may be controlled by changing the ratio of pitch to hole diameter. The SPP resonances we recover through Fourier transforms of the interferometric autocorrelations shed light on the classical problem of Fano interference in nanohole array extinction spectra.

© 2022 Author(s). All article content, except where otherwise noted, is licensed under a Creative Commons Attribution (CC BY) license (<http://creativecommons.org/licenses/by/4.0/>). <https://doi.org/10.1063/5.0082481>

Structured metallic surfaces may be utilized to couple free-space radiation to interfacial surface waves in the form of coherent charge density oscillations or surface plasmon polaritons (SPPs). SPPs represent a convenient method for transmitting optical signals over long distances at near light speeds with subwavelength mode confinement and have, therefore, been envisioned as a route to plasmon-assisted nanophotonic devices that surpass electronic analogues in speed and footprint.^{1–3} To date, a number of lithographically^{4–7} or ion-beam etched^{8–15} metallic and hybrid metal/dielectric¹⁶ structures have been used for this purpose. The SPP optical properties are principally determined by the coupler characteristics and metal dielectric constant. In this regard, two-dimensional plasmonic gratings (2PGs) comprised of periodic arrays of nanoholes are of particular interest for tailored SPP generation and manipulation given the sensitivity of the array optical properties to hole size, pitch, and geometry as has been amply demonstrated in the study of extraordinary optical transmission (EOT).^{17–22}

Early observations of EOT generated increased interest in the optical properties of SPPs in periodic systems, particularly in the

context of their dispersive spectral profiles.^{17,23} A body of research has dealt with the mechanisms underpinning the phenomenon and the various contributions to the asymmetric spectral features. Models proposed by Genet *et al.* and Sarrazin *et al.* around the same time explicitly considered direct (non-resonant) scattering and resonant SPP excitation channels.^{18,20} The first followed the Rayleigh wavelength and exhibited a sharp spectral transition. The second effect was a diffuse signature due to the excitation of surface waves, which are currently accepted as SPPs. The resulting Fano lineshapes are asymmetrical due to the coupled nature of these effects.²⁴ Similarly, Chang and coworkers used finite-difference time-domain (FDTD) simulations to model periodic arrays of nanoholes on gold surfaces. Their results indicate that coupling of a direct SPP-Bloch state to a continuum represented by the single-hole states is consistent with Fano's analysis, producing asymmetric line shapes.²²

Due to their coupled nature, continuum and hole contributions to nanohole array optical spectra cannot be directly decomposed. In addition, traditional optical transmission/reflection measurements

display peaks indicative of SPP formation from both the metal/air and metal/substrate interfaces although often these are spectrally separable.^{18,20,22,25,26} Our approach utilizes interferometric time-resolved photoemission electron microscopy (ITR-PEEM)^{11,12,27} measurements to uncouple the underlying direct SPP excitation at the air/metal interface from the optical Fano profile. Our current measurements take advantage of recently reported photoemission electron microscopy (PEEM) measurements at off-normal incidence,²⁸ which demonstrated that 2PGs may produce surface-bound SPPs that propagate in the direction opposite to the incident light field. In this configuration, due to the oppositely signed field and plasmon wave vectors, SPPs propagate and can be imaged without interference with the driving excitation laser field, which normally results in self-interference near-field emission patterns,^{10,12} as exemplified by normal incidence PEEM measurements.^{13,29,30} Ultrafast PEEM has been applied in various contexts for investigating the near-field response of plasmonic structures.^{10,12,27,31}

Here, we employ phase-locked, femtosecond pulse pairs in the counter-propagating geometry to launch SPPs from a series of lithographically patterned 2PGs with well-defined pitches and hole diameters. By tuning the time delay between the interferometrically locked pulses and a third higher energy probe pulse, we record linear SPP autocorrelation functions. The nonlinear photoemission images we record represent temporal snapshots of SPP–SPP interference, which we can directly relate to SPP spectral components through Fourier transforms. This analysis allows us to measure the SPP discrete resonances sustained by the arrays, and our approach may be utilized to isolate the propagating SPP resonance from the larger set of optical transitions (continuum) that contribute to the observed Fano resonances of periodically structured metallic surfaces. This analysis is carried out on a series of pitch-tuned 2PGs in both the co- and counter-propagating coupling regimes. In the counter-propagating direction, we show that tuning the array pitch near the fundamental plasmon resonance generates color-tuned narrow bandwidth SPPs. We also illustrate that the SPP bandwidths can be tuned by changing the ratio of pitch to hole diameter.

It is well appreciated that optical fields cannot be directly coupled to SPPs because of the small mismatch in momentum between free-space photon fields and coupled SPPs. This mismatch is on the order of a few percent at optical frequencies and is readily accomplished through scattering from surface structures such as individual holes or trenches.^{9,10,13,29,32} In contrast, 2PG couplers add additional tunable in-plane momentum as determined by the grating pitch. Our experiments utilize 2PG couplers of different pitches between 385 and 420 nm prepared by focused ion beam milling holes of varying diameters in a 15×15 square lattice configuration into 100 nm thick silver sputtered over freshly stripped mica.

Formally, the array contributes grating momentum $m * \mathbf{G}$, where \mathbf{G} is defined as $2\pi/a_0$, with a_0 being the hole spacing, and m is the order number. If the incident photon in-plane momentum summed with the grating momentum matches the SPP momentum, then a SPP will be launched from the array as given by

$$k_l * \sin(\alpha) \pm m\vec{G} = k_l * \sqrt{\frac{\epsilon(\lambda)}{1 + \epsilon(\lambda)}}, \quad (1)$$

where α is the incident angle measured relative to the surface normal, k_l is the input laser wave vector, and $\epsilon(\lambda)$ is the bulk dielectric constant.

At normal incidence, there are two solutions corresponding to plus and minus first order diffraction. These SPPs are degenerate in energy and produce a standing wave Bloch solution within the array. As the angle differs from normal incidence, the plus–minus degeneracy is lifted and results in SPPs traveling in both the co- and counter-propagating directions with different wave vectors. At our excitation wavelength of 785 nm and angle of incidence near 75° , the grating pitch needed for positive order SPP excitation is $\sim 15 \mu\text{m}$ while the grating pitch needed for the negative order SPP is $\sim 395 \text{ nm}$ (see the [supplementary material](#)). Once launched by the array, the SPPs propagate along the surface subject to the real and imaginary parts of the metal surface dielectric.

Optical reflectivity spectra recorded on our 2PGs reveal complex asymmetric lineshapes with features that tune and shift with grating period (see [supplementary material](#) Fig. S1). As mentioned above, similar features observed in transmission mode extinction spectroscopy have been associated with the continuum + discrete Fano model.^{18,20,22}

The existence of a counter-propagating SPP on the air/metal interface allows de-convolution of the Fano line shape and measurement of the air/metal interface SPP contribution corresponding to the direct state in the Fano model. To accomplish this, we utilize two-color ITR-PEEM to obtain SPP time profiles and then Fourier transform the profiles to obtain the SPP spectra. [Figure 1\(a\)](#) outlines the principle of two-color ITR-PEEM correlation measurements. A phase-locked pair of 785 nm, 15 fs pulses emanating from a Ti:sapphire oscillator operating at 90 MHz serve as SPP preparation pulses. In addition, a separate non-phase stabilized blue pulse ($\sim 392 \text{ nm}$, 90 fs) produced through second harmonic generation of a portion of the Ti:sapphire output is routed collinearly with the SPP preparation pulses to facilitate two-photon photoemission. All pulses are p -polarized and impinge on the sample with an incidence angle of $\sim 75^\circ$. Under near-grazing incidence, the incident pulse spatial profiles are elliptical and while the focused pump pulse pair is primarily centered on the 2PG, the secondary blue pulse is expanded to encompass the entire $150 \mu\text{m}$ field-of-view [[Fig. 1\(a\)](#)].

Our experiments utilize a 400 nm pitch 2PG, which enables pairwise excitation of counter-propagating SPPs at the pump wavelength of 785 nm. In a typical single-color ITR-PEEM experiment, the photoelectron yield recorded as a function of delay between the pulses generates a time profile interferogram through the coherent interaction of the phase-locked pump and probe beams with the metal surface. The interferogram displays peaks and valleys depending on the relative phase difference between the excitation pulse fields. We have previously shown that using a harmonic of the excitation wavelength as a probe suppresses the field oscillations leading to a signal that only depend on the carrier envelope cross correlation.³³ This is clear in [Fig. 1\(b\)](#), which shows PEEM images of the SPP pair at several time delays. The SPP fields appear as isolated Gaussian envelopes labeled P_{1SPP} and P_{2SPP} in [Fig. 1](#). The coarse spatial positioning of the field envelopes relative to the 2PG coupler is controlled by time delay of the blue (P_3) harmonic field. Interferogram acquisition involves scanning the relative phase delay of a single (800 nm) pulse-initiated SPP [P_{1SPP} , [Fig. 1\(b\)](#)] while the blue (400 nm) pulse delay and position of the reference (800 nm) SPP (P_{2SPP}) are fixed. Near the phase delay corresponding to temporal overlap between P_{1SPP} and P_{2SPP} , the SPP fields interact interferometrically yielding clear temporal oscillations of the Gaussian envelope intensity as shown in [Fig. 1\(d\)](#). Note, at the same time delay, the 800 nm phase-stabilized pump fields also interfere leading to

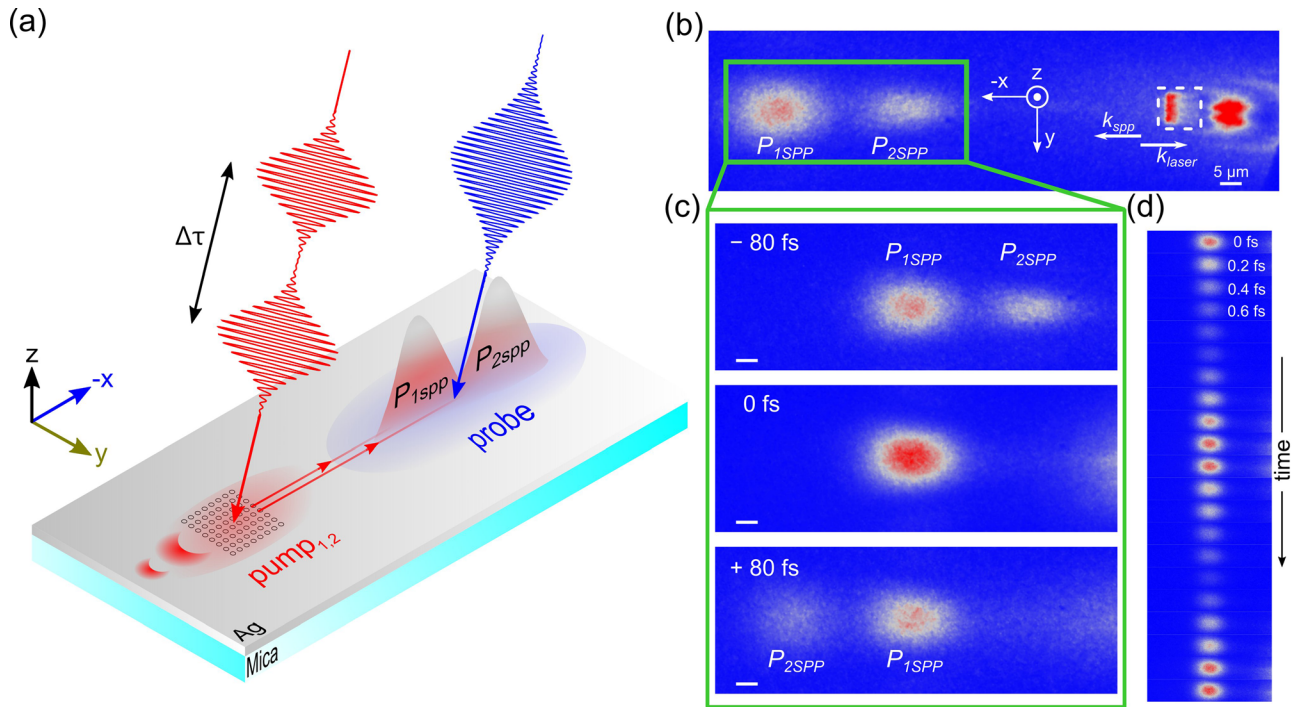


FIG. 1. 2PG enabled bi-directional SPP launching and ITR-PEEM imaging. (a) Schematic of the experimental configuration for co- and counter-propagating SPP imaging. (b) Intensity map of interferometrically locked counter-propagating SPPs (P_{1SPP} , P_{2SPP}). (c) PEEM images at various relative time delays between P_{1SPP} and P_{2SPP} during auto-correlation acquisition (top: -80 fs, middle: 0 fs, bottom $+80$ fs). When the SPPs temporally overlap, field interference can be observed. This is shown in (d) where each panel corresponds to a 0.2 fs time step beginning with a 0 fs relative time delay between the SPPs.

temporal oscillations. The large spatial offset between the 2PG origin and the SPP positions allows us to isolate these responses.

Interferograms were acquired on a series of pitch-tuned 2PGs by spatially integrating the P_2 signal area of the PEEM image as the P_1 phase is scanned over a range of ~ 200 fs in 0.2 fs steps. The results are shown in Fig. 2(a). In these measurements, the hole size was kept constant at 100 nm, and the pitch was varied between 370 and 430 nm. The ITR-PEEM interferograms may be related to fundamental polarization fields by recognizing that in the two-color interferometric time-resolved PEEM measurements, the photoelectron yield, S , may be written as

$$S(\vec{r}) \propto \int_{-\infty}^{\infty} \left| \sum_i P_i(\vec{r}, t) \right|^{2n} dt, \quad (2)$$

where $P_i(\vec{r}, t)$ represents the i th contribution to the total nonlinear polarization and n is the order of the process, determined by the minimum number of photons needed to exceed the work function threshold in the material. In our experimental configuration, the silver work function dictates that a second order process involving one red and one blue photon dominates photoemission.³³ The resulting delay-dependent signal may be expressed as

$$\begin{aligned} S(x, \tau) \propto \int_{-\infty}^{\infty} dt & \left[C_1 * P_1(x, t) \cdot P_2^*(x, t + \tau) \right. \\ & + C_2 * P_1(x, t) \cdot P_{2SPP}^*(x, t + \tau) + C_3 * P_{1SPP}(x, t) \\ & \cdot P_2^*(x, t + \tau) + C_4 * P_{1SPP}(x, t) \cdot P_{2SPP}^*(x, t + \tau) \\ & \left. \cdot P_3(x, t) \cdot P_3^*(x, t) + c.c. \right] \end{aligned} \quad (3)$$

where x is the propagation direction [see Fig. 1(a)] and P_1 , P_2 , and P_3 are the input laser field-induced polarizations due to the red pump (P_1 , P_2) and blue interrogation (P_3) fields. P_{iSPP} is the corresponding SPP polarization fields, τ is the delay time between the two 785 nm red laser pulses, and a star indicates the field complex conjugate. C_i are proportionality constants, and c.c. denotes the complex conjugate. The first term is the excitation-field/excitation-field correlation term. The second and third terms are related to excitation field-plasmon cross correlation, which give rise to spatial interference familiar to the co-propagating geometry.^{10,12,13} The final term in the integrand appearing in brackets is the plasmon-plasmon correlation of interest. We separate these terms by making use of the spatial and temporal separation between plasmon and excitation field(s) (see Fig. S2).

The raw interferograms given in Fig. 2(a) mimic linear Gaussian pulse autocorrelations, which contain the frequency components of the launched SPPs. The SPPs travel in the counter-propagating direction in space with increasing time delay, and the initiating fields travel in the co-propagating direction in space with increasing time delay. Therefore, the SPP and initiating fields only temporally and spatially overlap and, thus, interfere in the region at and immediately surrounding the 2PG spatial origin. Beyond this region, the SPP is spatially isolated and may be readout through concurrent interaction with the temporally overlapped blue field (P_3). By spatially and temporally isolating the linear SPP-SPP autocorrelation term in Eq. (3), the measured interferograms may be directly related to SPP spectra through their Fourier transforms as given in Fig. 2(b).

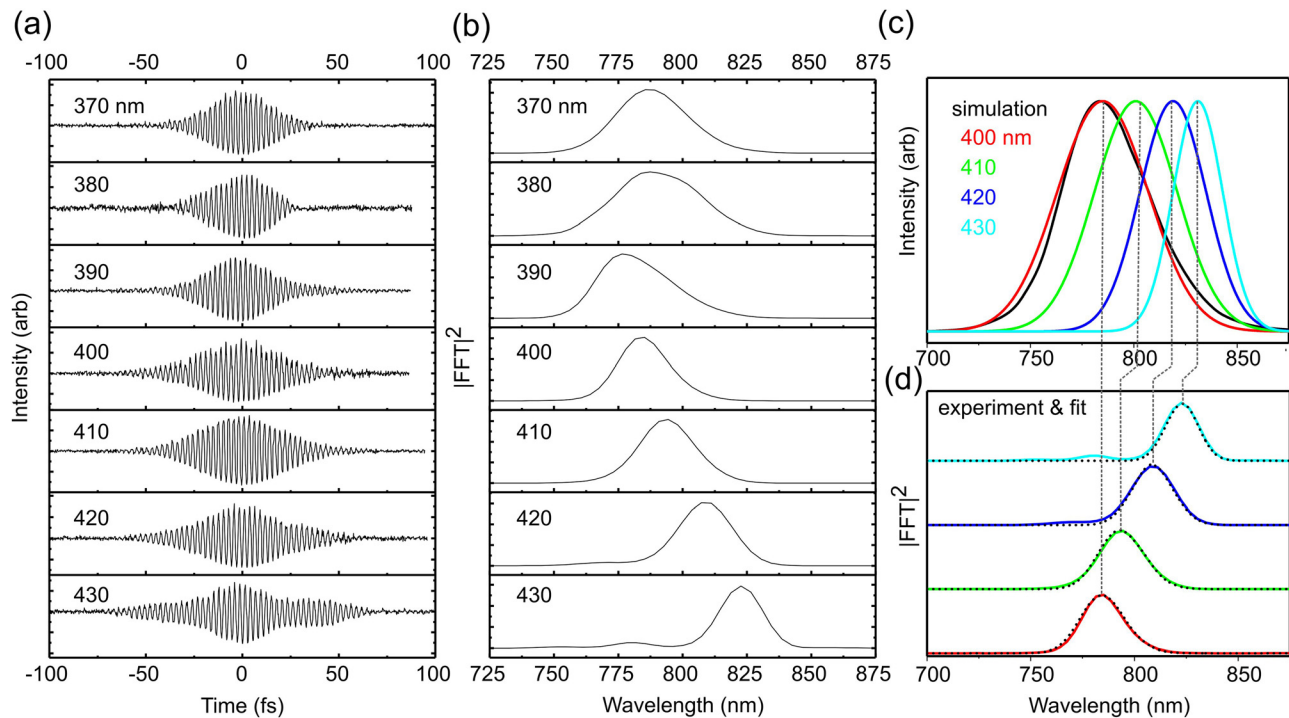


FIG. 2. Surface plasmon linear autocorrelation and spectroscopy. (a) Interferograms recorded through ITR-PEEM on a series of 2PG-initiated SPPs with pitches between 370 (top) and 430 nm (bottom). (b) SPP spectra recovered through the Fourier transform of the interferograms presented in (a). (c) Simulated array resonances for the 400–430 nm pitch series and excitation source spectrum (black trace). The frequency domain product of the array resonances and source spectrum gives rise to the experimentally observed SPP spectra shown in (d) along with fits of the same (dotted traces).

For 2PG pitches > 390 nm, the SPP spectral center wavelengths monotonically redshift over the ~ 780 – 825 nm range and spectrally narrow. For 2PG pitches < 390 nm, the spectra gradually tend to a fixed frequency of 775 nm and concomitantly broaden as the pitch decreases. At a pitch of about 390 nm, the SPP bandwidth is essentially identical to the source. The measured SPP spectra correspond to 2PG grating resonances that are windowed by the bandwidth of pump laser. In order to extract the 2PG resonant coupling spectrum, we first identify the free-space wavelength that solves Eq. (1) for a given array period. This condition can be true for one free-space central wavelength for a given 2PG pitch and excitation angle, because Eq. (1) is an implicit function of the excitation wavelength. For a pitch of 400 nm, this wavelength is ~ 780 nm, near the center of our excitation pulse.

The simulated 2PG resonant coupling spectra are modeled as Gaussians centered at the wavelengths determined uniquely by the criteria described above. Since the 2PG resonance center wavelength is fixed by k_{SPP} , the only adjustable parameter is the 2PG resonance bandwidth. This analysis determines the 2PG grating resonances, which are shown in Fig. 2(c) for the 400–430 nm pitch arrays. The fitted spectra are shown in Fig. 2(d) for the 2PG of pitch 400 nm and above along with the simulated array resonances and pump pulse spectrum. Since the source bandwidth is fixed, the 2PG spectrum central wavelength quickly moves beyond the available source wavelengths. At this point, any coupling between the source and the SPP must occur in the wings of both spectra, which ultimately decreases the coupling strength. We note that the incident source is essentially

responsible for the limited tuning range using the 2PG coupler. Utilizing a broader bandwidth source would result in a larger tuning shift.

For 2PGs with pitch < 390 nm, there is a noticeable broadening of the SPP spectra without significant change in the spectrum center wavelength. Significantly broader 2PG resonances must be used to simulate the recorded SPP spectra in this region. Thus, as the hole diameter to pitch ratio increases, the 2PG resonance becomes significantly broader. At this point, the 2PG acts as a broadband coupler and the SPP becomes a wavelength-shifted near copy of the source spectrum. In Fig. 3, we show results from 2PGs with pitch 380 nm but with three different hole sizes. Increasing the hole diameter for a constant pitch results in red-shifting and broadening of the SPP spectra. The SPP frequencies tune over a narrow range, reaching the pump pulse center frequency in the case of 125 nm holes. For the smallest hole diameter 2PG (75 nm), the linewidth of 36 nm FWHM agrees with the linewidth for a 400 nm pitch, 100 nm hole diameter array [Fig. 2(b)]. Increasing the hole diameters leads to uncertainty in pitch, which influences the wave vector distribution sustained by the arrays through the spatial extent of the periodic field distribution, in effect, broadening the spectra. In the same way, a distribution of hole sizes would also contribute to spectral broadening.

The systematics of the hole size parameter are commonly addressed through zero-order, normal incidence transmission measurements, which produce the Fano profiles discussed above. Changes in the magnitude and displacement of the transmission features with

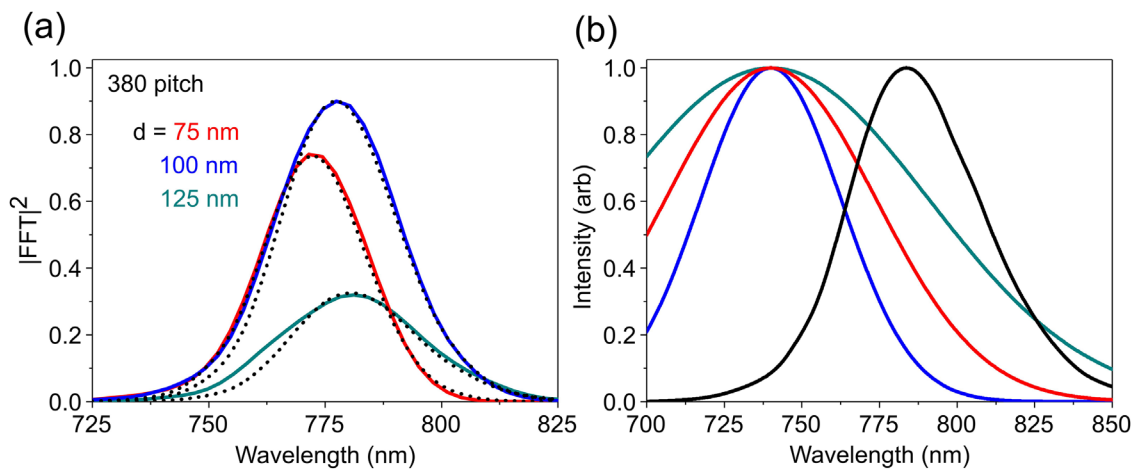


FIG. 3. (a) SPP spectra acquired on a series of 380 nm pitch 2PGs with varying hole diameters (d) and simulated spectra (dotted traces). (b) Recovered array resonances and source excitation spectrum (black).

varying hole sizes are typically associated with the frequency-dependent scattering efficiency of the isolated hole continuum state.²² While this interpretation is commonly invoked to rationalize red-shifting of the Fano profiles with increasing hole diameter, the 2PG resonances presented in Figs. 2 and 3 suggest that variations in the surface polariton resonance linewidths with hole diameter or pitch also contribute to the observed red shifting. The magnitude of the variations observed here suggests the effect is pronounced, and the 2PG resonance linewidths and isolated hole scattering cross sections influence the Fano profile cooperatively. Importantly, the ITR-PEEM based SPP linear autocorrelation method employed herein solely addresses the propagating air/metal interfacial SPP component of the 2PG excitation and, therefore, may be distinguished from conventional transmission and/or reflection spectroscopies, which interrogate the coupled system of holes and SPPs propagating within the array. While this analysis recovers the wavelength components of resonantly coupled SPP via counter-propagation, complementary measurements recorded in the co-propagating direction recover SPP spectra that are closely related to the excitation laser spectrum (see the [supplementary material](#)). Here, the 2PG-derived co-propagating SPPs arise as a result of scattering from individual holes.

In conclusion, we presented an approach to measuring the autocorrelation of surface plasmons directly resulting in the determination of the coupling structure resonance without interference from continuum hole scattering states that give rise to Fano profiles in the optical extinction spectra. The results from a series of nanohole arrays of varying pitches and hole diameters demonstrated that the SPP wavelength can be tuned from approximately 770 to 820 nm. In addition, the 2PG-coupled SPP spectra show an increasing bandwidth with a smaller pitch wavelength, a result that maps the array resonance itself. This is interpreted as increasing momentum uncertainty as the hole diameter approaches the hole spacing. Similar measurements on co-propagating SPPs demonstrate that the autocorrelation technique may be used to experimentally determine coupling structure resonances analogous to the counter-propagating case.

See the [supplementary material](#) for 2PG optical reflectivity spectra and co-propagating SPP autocorrelation results.

The authors acknowledge support from the U.S. Department of Energy (DOE), Office of Science, Office of Basic Energy Sciences, Division of Chemical Sciences, Geosciences and Biosciences. This work was performed in EMSL, a National Scientific User Facility sponsored by DOE's Office of Biological and Environmental Research and located at PNNL. PNNL is operated by Battelle Memorial Institute for the United States Department of Energy.

AUTHOR DECLARATIONS

Conflict of Interest

The authors have no conflicts to disclose.

DATA AVAILABILITY

The data that support the findings of this study are available from the corresponding authors upon reasonable request.

REFERENCES

- ¹R. Kirchain and L. Kimerling, "A roadmap for nanophotonics," *Nat. Photonics* **1**, 303 (2007).
- ²E. Ozbay, "Plasmonics: Merging photonics and electronics at nanoscale dimensions," *Science* **311**, 189 (2006).
- ³W. L. Barnes, A. Dereux, and T. W. Ebbesen, "Surface plasmon subwavelength optics," *Nature* **424**, 824 (2003).
- ⁴Z. Hirboodvash, M. Khodami, N. R. Fong, E. Lisicka-Skrzek, A. Olivieri, H. Northfield, R. Niall Tait, and P. Berini, "Grating couplers fabricated by e-beam lithography for long-range surface plasmon waveguides embedded in a fluoropolymer," *Appl. Opt.* **58**, 2994 (2019).
- ⁵R. Zia and M. L. Brongersma, "Surface plasmon polariton analogue to Young's double-slit experiment," *Nat. Nanotechnol.* **2**, 426 (2007).
- ⁶T. Tanemura, K. C. Balram, D. S. Ly-Gagnon, P. Wahl, J. S. White, M. L. Brongersma, and D. A. Miller, "Multiple-wavelength focusing of surface plasmons with a nonperiodic nanoslit coupler," *Nano Lett.* **11**, 2693 (2011).
- ⁷I. P. Radko, S. I. Bozhevolnyi, A. B. Evlyukhin, and A. Boltasheva, "Surface plasmon polariton beam focusing with parabolic nanoparticle chains," *Opt. Express* **15**, 6576 (2007).

- ⁸Y. Gong, A. G. Joly, P. Z. El-Khoury, and W. P. Hess, "Interferometric plasmonic lensing with nanohole arrays," *J. Phys. Chem. Lett.* **5**, 4243 (2014).
- ⁹Y. Gong, A. G. Joly, P. Z. El-Khoury, and W. P. Hess, "Nonlinear photoemission electron micrographs of plasmonic nanoholes in gold thin films," *J. Phys. Chem. C* **118**, 25671 (2014).
- ¹⁰Y. Gong, A. G. Joly, D. Hu, P. Z. El-Khoury, and W. P. Hess, "Ultrafast imaging of surface plasmons propagating on a gold surface," *Nano Lett.* **15**, 3472 (2015).
- ¹¹A. Kubo, K. Onda, H. Petek, Z. Sun, Y. S. Jung, and H. K. Kim, "Femtosecond imaging of surface plasmon dynamics in a nanostructured silver film," *Nano Lett.* **5**, 1123 (2005).
- ¹²A. Kubo, N. Pontius, and H. Petek, "Femtosecond microscopy of surface plasmon polariton wave packet evolution at the silver/vacuum interface," *Nano Lett.* **7**, 470 (2007).
- ¹³L. Zhang, A. Kubo, L. Wang, H. Petek, and T. Seideman, "Imaging of surface plasmon polariton fields excited at a nanometer-scale slit," *Phys. Rev. B* **84**, 245442 (2011).
- ¹⁴L. Yin, V. K. Vlasko-Vlasov, J. Pearson, J. M. Hiller, J. Hua, U. Welp, D. E. Brown, and C. W. Kimball, "Subwavelength focusing and guiding of surface plasmons," *Nano Lett.* **5**, 1399 (2005).
- ¹⁵A. Bouhelier, T. Huser, H. Tamaru, H. J. Güntherodt, D. W. Pohl, F. I. Baida, and D. Van Labeke, "Plasmon optics of structured silver films," *Phys. Rev. B* **63**, 155404 (2001).
- ¹⁶H. Zhang, B. Abhiraman, Q. Zhang, J. Miao, K. Jo, S. Roccasecca, M. W. Knight, A. R. Davoyan, and D. Jariwala, "Hybrid exciton-plasmon-polaritons in van der Waals semiconductor gratings," *Nat. Commun.* **11**, 3552 (2020).
- ¹⁷H. F. Ghaemi, T. Thio, D. E. Grupp, T. W. Ebbesen, and H. J. Lezec, "Surface plasmons enhance optical transmission through subwavelength holes," *Phys. Rev. B* **58**, 6779 (1998).
- ¹⁸C. Genet, M. P. van Exter, and J. P. Woerdman, "Fano-type interpretation of red shifts and red tails in hole array transmission spectra," *Opt. Commun.* **225**, 331 (2003).
- ¹⁹L. Salomon, F. Grillot, A. V. Zayats, and F. de Fornel, "Near-field distribution of optical transmission of periodic subwavelength holes in a metal film," *Phys. Rev. Lett.* **86**, 1110 (2001).
- ²⁰M. Sarrazin, J.-P. Vigneron, and J.-M. Vigoureux, "Role of wood anomalies in optical properties of thin metallic films with a bidimensional array of subwavelength holes," *Phys. Rev. B* **67**, 085415 (2003).
- ²¹S. A. Darmanyan and A. V. Zayats, "Light tunneling via resonant surface plasmon polariton states and the enhanced transmission of periodically nanostructured metal films: An analytical study," *Phys. Rev. B* **67**, 035424 (2003).
- ²²S.-H. Chang, S. K. Gray, and G. C. Schatz, "Surface plasmon generation and light transmission by isolated nanoholes and arrays of nanoholes in thin metal films," *Opt. Express* **13**, 3150 (2005).
- ²³T. W. Ebbesen, H. J. Lezec, H. F. Ghaemi, T. Thio, and P. A. Wolff, "Extraordinary optical transmission through sub-wavelength hole arrays," *Nature* **391**, 667 (1998).
- ²⁴U. Fano, *J. Opt. Soc. Am.* **31**, 213 (1941).
- ²⁵J. M. McMahon, J. Henzie, T. W. Odom, G. C. Schatz, and S. K. Gray, "Tailoring the sensing capabilities of nanohole arrays in gold films with Rayleigh anomaly-surface plasmon polaritons," *Opt. Express* **15**, 18119 (2007).
- ²⁶J. Prikulis, P. Hanarp, L. Olofsson, D. Sutherland, and M. Käll, "Optical spectroscopy of nanometric holes in thin gold films," *Nano Lett.* **4**, 1003 (2004).
- ²⁷C. Lemke, T. Leißner, S. Jauernik, A. Klick, J. Fiutowski, J. Kjølstrup-Hansen, H.-G. Rubahn, and M. Bauer, "Mapping surface plasmon polariton propagation via counter-propagating light pulses," *Opt. Express* **20**, 12877 (2012).
- ²⁸K. T. Crampton, A. G. Joly, and P. Z. El-Khoury, "Direct visualization of counter-propagating surface plasmons in real space-time," *J. Phys. Chem. Lett.* **10**, 5694 (2019).
- ²⁹P. Kahl, D. Podbiel, C. Schneider, A. Makris, S. Sindermann, C. Witt, D. Kilbane, M. Horn-von Hoegen, M. Aeschlimann, and F. Meyer zu Heringdorf, "Direct observation of surface plasmon polariton propagation and interference by time-resolved imaging in normal-incidence two photon photoemission microscopy," *Plasmonics* **13**, 239 (2018).
- ³⁰P. Kahl, S. Wall, C. Witt, C. Schneider, D. Bayer, A. Fischer, P. Melchior, M. Horn-von Hoegen, M. Aeschlimann, and F.-J. Meyer zu Heringdorf, "Normal-incidence photoemission electron microscopy (NI-PEEM) for imaging surface plasmon polaritons," *Plasmonics* **9**, 1401 (2014).
- ³¹H. Hu, Y. Qin, P. Lang, X. Song, B. Ji, and J. Lin, "Investigation of a dual-hole structure-based broadband femtosecond nondiffracting SPP beam emitter by photoemission electron microscopy," *Opt. Laser Technol.* **146**, 107538 (2022).
- ³²B. Sun, B. Ji, P. Lang, Y. Qin, and J. Lin, "Local near-field optical response of gold nanohole excited by propagating plasmonic excitations," *Opt. Commun.* **505**, 127498 (2022).
- ³³A. G. Joly, P. Z. El-Khoury, and W. P. Hess, "Spatiotemporal imaging of surface plasmons using two-color photoemission electron microscopy," *J. Phys. Chem. C* **122**, 20981 (2018).